Energy loss during air flow through biofilter media

- Impact of entrance region minor loss, biomass accumulation and media characteristics

By Røskva Lill Lindgård Høimark

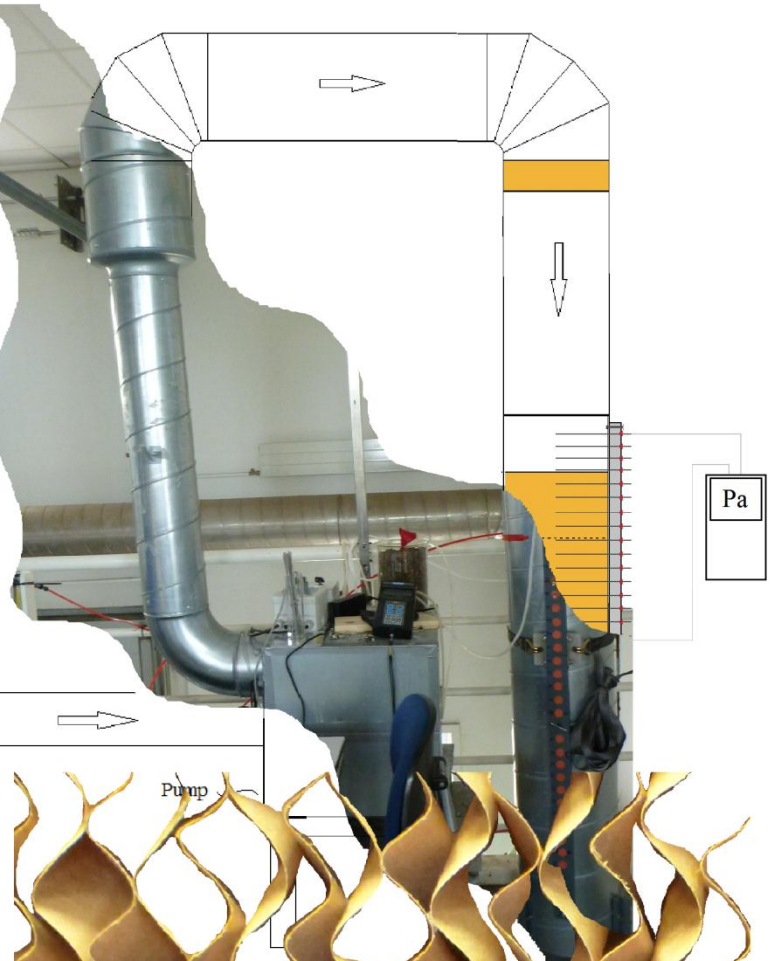

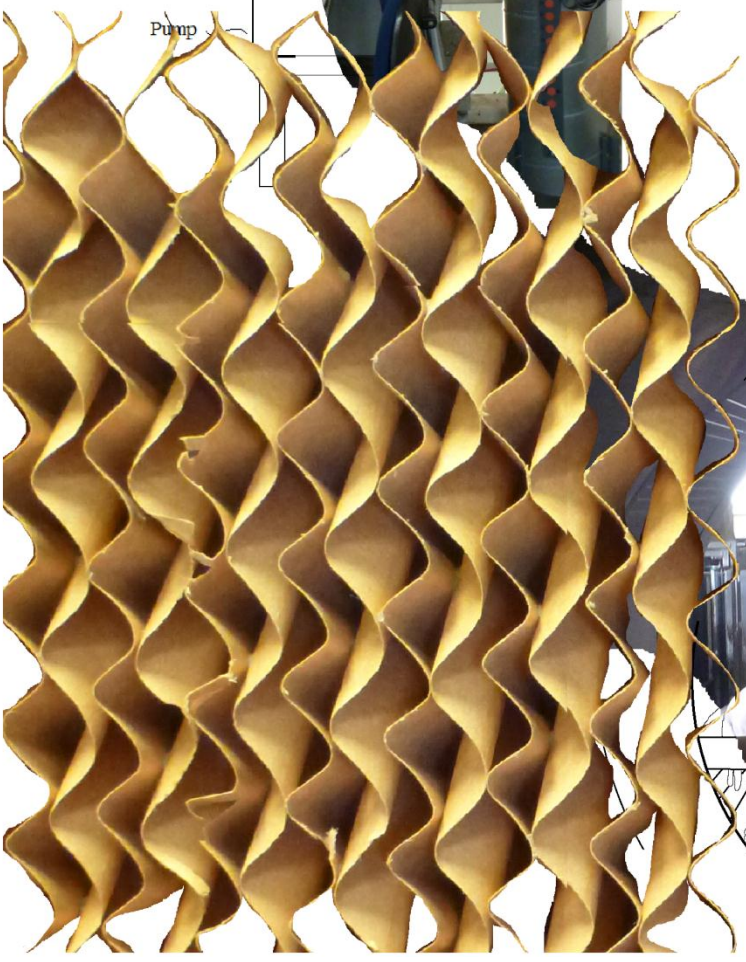

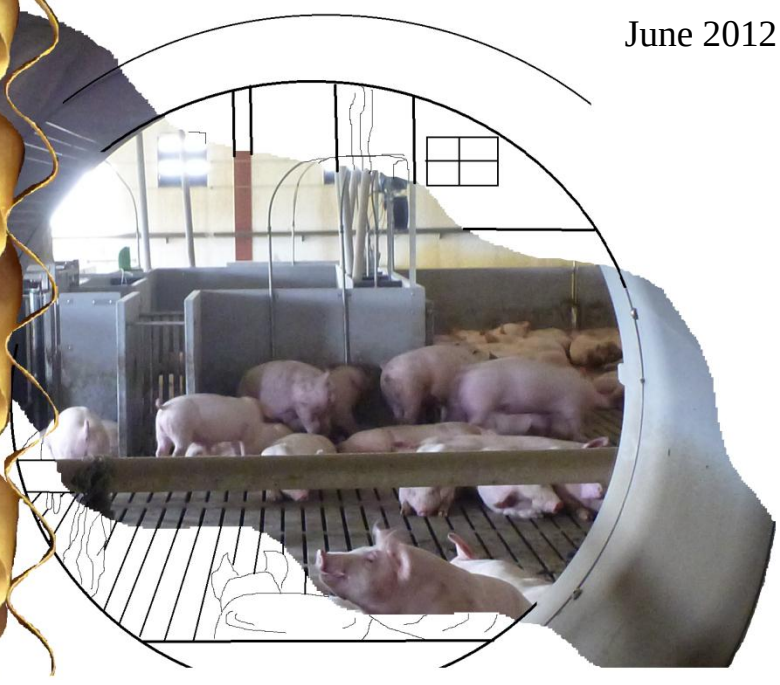

K10M-project

Section of Environmental Engineering

Department of Biotechnology, Chemistry and Environmental Engineering

Aalborg University

June 2012

English title:
Energy loss during air flow through biofilter media - Impact of entrance region minor loss, biomass accumulation and media characteristics

Dansk titel:
Energitab ved luft flow gennem biofilter medier - Betydning af enkelt tab på forkanten af filteret, akkumulering af biomasse samt medie karakteristika.

Project type: Master Thesis

Project Period: February 1^{st} 2012 - June 15^{th} 2012

Author:

Røskva Lill Lindgård Høimark

Supervisors:

Tjalfe Gorm Poulsen
Associate professor at Department of Biotechnology, Chemistry and Environmental Engineering, Aalborg University

Rune Røjgaard Andreasen
Ph.d student at Department of Biotechnology, Chemistry and Environmental Engineering, Aalborg University

Editions: 4

Number of Pages: 51
- Report: 48
- Appendix: 3

Additional Material: CD-ROM

AALBORG UNIVERSITET

Preface

This report was done at Aalborg University (Denmark) in cooperation with the company SKOV A/S as a part of the Master program in Environmental Engineering.

I would like to present a great thanks to my supervisors Tjalfe Poulsen and Rune Røjgaard Andreasen for the help and support through out my project.

Furthermore I thank Niels Riis and Lise Bonne Guldberg for making the cooperation with SKOV A/S possible, for providing filter materials for the experiments and for the opportunity to test an active Munters biofilter at the test facility on Mors.

Throughout the report references from books, articles and homepages will appear with the last name of the author and the year of publication in the form of [Author, Year]. They can also appear with specific reference to a chapter, page, figure or table.

Figures and tables in the report are numbered according to the respective chapter. In this way the first figure in chapter three is number 3.1, the second is number 3.2 and so on. Figure and table captions are given below each figure and above each table respectively.

The different excel sheets containing the data and calculations for this project are given in appendix.

Abstract

The focus of the project is to identify and quantify the minor energy losses over the entry and exit during gas flow through biofilter materials. The investigation, of minor loss dependency on biofilter medium characteristics and flow conditions, was carried out using five different laboratory scale biofilter units.

For this purpose the gas pressure variation across the different filter units were measured for a range of different gas flow velocities, before the inlet, inside and after the outlet of the filter units.

The measurements showed that filter material characteristics such as pore size and pore orientation have a significant impact on the pressure variation across the filter units.

In addition the variations in gas energy level across the filter units was measured and successfully modelled.

The modelling confirmed that both pore size and pore orientation have a significant influence on the minor energy losses over the inlet of the filter.

Additional measurements of pressure loss were carried out on a full scale biofilter unit located at a pig production facility.

The result showed that the presence of a biofilm inside the biofilter material can have a very significant impact on the pressure loss. In general pressure loss increase rapidly with increasing biofilm thickness. The results also showed that biofilm density within the biofilter material varies with location, but is generally higher near the inlet.

In conclusion this project shows that there exist minor pressure and energy losses over the inlet and outlet of biofilter media (something that has not previously been documented) and that it is possible to model these losses.

Resume

Fokusset i dette projekt er, at identificere og kvantificere enkelttabene og energitabene henover ind-og udløbet af forskellige biofilter med forskellige luft flow. Undersøgelsen af enkelt-tab afhængighed af biofiltre medies karakteregenskaber og flow betingelser, hvilke blev udført ved brug af fem forskellige laboratorieskala biofilterenheder.

Til dette formål var trykvariationen henover de forskellige filterenheder målt før indløbet, indeni filteret og efter udløbet, under en række forskellige strømningshastigheder.

Målingerne viste, at filtermaterialets egenskaber, såsom porestørrelse og pore retning har en signifikant indflydelse på trykvariation henover filterenheden.

Endvidere blev variationer i gas-energi niveau henover filterenhederne målt og blev med succes modelleret.

Modelleringen bekræftede, at både porestørrelsen og pore retningen har en signifikant indflydelse på enkelt-energitabene henover indgangen til filterene.

Yderligere blev tryktabets målinger udført på en fuldskala biofilterenhed placeret ved et svineproduktionsanlæg.

Resultaterne viste, at tilstedeværelsen af biofilm indeni biofilter materialet kan have en signifikant indvirkning på tryktabet, som generelt set falder hurtig med stigende biofilm tykkelse. Resultaterne viste også, at biofilm densiteten indeni biofilteret varierer efter placering, men er generelt højere nær indløbet.

Der konkluderes, at der findes enkelt-tryktab og energitab henover ind- og udløbet af biofilter medier (noget, der ikke tidligere er blevet dokumenteret), og at det er muligt at modellere disse tab.

Table of contents

Introduction 1

Denmark produces about 25 million pigs annually [Lyngbye et al., undated]. These productions takes place at large production facilities in which large numbers of animals are located in a small area [Schiffman et al., 1994]. During production, large amount of air have to be ventilated to remove heat and gaseous contaminants. For example a maximum ventilation requirements for a finishing piggery with 250 pigs at 90 kg is 171.2 $m^3/(h \cdot Animal)$ [O'Neill et al., 1992].

Many of the gaseous contaminants are strongly odorous and give rise to odour problems in the surroundings [O'Neill et al., 1992].

Odour problems from livestock production can be an important issue for the surroundings [Dansk Landbrugsrådgivning, undated]. Animal production has over the recent decades been concentrated at fewer and larger production units resulting in very significant odour problems for their surroundings. There is therefore an increasing pressure to find technical solutions to reduce odour emissions [Schiffman et al., 1994].

In the law according to environmental approval of livestock (nr. 1572 from 20/12/2006) do livestock farms have to prevent and reduce the odour nuisance with respect to its neighbours [Dansk Landbrugsrådgivning, undated]. It is therefore essential to implement odour control methods if the production level at an animal farm is to be maintained or increased [Lyngbye et al., undated].

Key requirements for odour removal technology is that it must be cost-effective and relatively easy to maintain and operate in order to avoid excessive increases in animal production costs [Lyngbye et al., undated]. Cleaning costs are important as higher production prices per pig will affect sales and exports, resulting in decreasing income for the farmer [Lyngbye et al., undated]. Excessively high costs may result in the pig production being moved to countries with lower production costs and fewer environmental regulations [Lyngbye et al., undated]. It is therefore important to develop odour removal methods that are cost-effective and easy to operate for the farmers.

Technologies for odour emission control at livestock production facilities are under continuous development both nationally and internationally [Riis et al., 2006].

Biofiltration is a technology that is receiving increasing attention as it is relatively low in cost and potentially very effective [Delhoménie et al., 2003]. It is used for air pollution control in connection with an increasing variety of industrial processes [Delhoménie et al., 2003]. In Europe biofiltration is a widely used waste-air control technology and during recent years use of this technology has it also increased in United States [Schwarz et al., 2001].

Biofiltration involves passing the contaminated gas stream through a wetted fixed-bed

reactor containing a porous medium that supports the growth of microbial biomass typically in form of a biofilm [Schwarz et al., 2001]. The gas phase contaminants, which are pumped through the biofilter, are degraded in the biofilm [Schwarz et al., 2001].

The air flow characterises of the biofilter bed depend on the biofilter media. An ideal biofilter medium will have a high surface area for biofilm growth, long-term physical stability, low pressure drop, good moisture retention, pH buffering capacity and nutrients [Shareefdeen and Singh, 2005]. Both natural and inert materials can be used as biofilter media. Traditional natural media, which are used in simple biofilters, can be compost, peat, wood chips, straw and soil [Shareefdeen and Singh, 2005].

Natural materials for biofilters, like soil, compost or bark, are easily compacted, resulting in reduced pore spaces and large pressure loss [Schwarz et al., 2001]. Inert materials can have a greater bed porosity and pore size, because the inert materials do not degrade or compact easily, this give lower pressure losses and it make the material more preferable as they become cheaper in operational costs [Macdonald et al., 1979]. Examples of inert media can be lava rock, polyurethane foam cubes (PUF), Pall rings, porous ceramic beads and porous ceramic Raschig rings [Kim and Deshusses, 2008].

Biofiltration is a relatively low cost technology [Delhoménie et al., 2003] and a reliable method for cleaning off-gas streams, with large flow rates and low contaminant concentrations [Schwarz et al., 2001]. It is therefore competitively advantageous in comparison with traditional processes, such as chemical scrubbing, activated carbon adsorption and incineration [Delhoménie et al., 2003].

The costs of biofiltration are generally split into two parts: construction and operations/maintenance costs [Chin and Hoff, 2009]. The parameters, which control the cost efficiency, are the energy consumption in the filter and the decomposition efficiency. These are further depending on the media characteristics, the flow velocity and the biofilter geometry, which all effect the pressure drop over the filter [Schwarz et al., 2001] [Macdonald et al., 1979].

The pressure drop is therefore directly controlling the energy comsumption. It is therefore one of the most important parameters to understand.

At present biofilter pressure drop is known to depend on both biofilter geometry, flow velocity and filter media characteristics. It is generally assumed that the pressure decreases linearly with filter depth in filters consisting of homogeneous media [Trussell and Chang, 1999]. Recent observations, however indicate that this assumption is not completely correct as the pressure gradient across a given filter medium has been observed to vary with filter depth [Minelgaite et al., 2012]. As this non-linearity is not included in any of the generally applied equations for modelling biofilter pressure drop, it constitutes an unknown variable, when designing biofilters, and it is therefore relevant to investigate it in more detail.

Project aim 2

The purpose of this study is to carry out a more thorough measurement and analysis program for analysis of the pressure variations inside a biofilter than has been previously done. This includes the deviations from linearity as well as the parameters controlling the shape of the pressure-filter depth curve.

To assess the pressure loss inside a biofilter as a function of the filter depth a homogeneous artificial filter material will be used. This material is produced by Munters AB, Sweden, and used in humidifying and air cleaning applications by SKOV A/S Denmark. This material was chosen as it is readily available, comes in different thicknesses and pore geometries allowing for assessment of filter material property effects on pressure loss.

The Munters filter is made of special impregnated cellulose fibers with rot prevention and water absorption capability [SKOV A/S, undated] and is a material with high durability and low pressure loss.

Analyses will be carry out under controlled laboratory conditions using the filter materials with different pore sizes and different pore geometries for a range of different flow velocities.

Based on the measured pressure data an assessment of the energy conversion inside the biofilter material as well as the relationship between energy level, pressure level and biofilter material properties will be made.

Additional analyses on a full-scale operating biofilter will be carried out to assess the possibility of measurements under practical conditions as well as the impact of biomass in the filter on the pressure drop.

Theory 3

This chapter presents the theoretical background for the processes investigated in this project.

3.1 Flow and pressure loss in homogeneous porous media

Transport of fluids through porous media under conditions, where the flow is laminar and the effects of inertial forces are negligible, is often described by Darcy's law, which assumes that the pressure gradient is linearly proportional to the fluid velocity [Zeng and Grigg, 2006].

$$-\frac{\Delta P}{L} = \frac{\mu}{k_a} \cdot V \tag{3.1}$$

- ΔP = Pressure drop across the medium [Pa]
- L = Length of medium [m]
- k_a = Air permeability [m^2]
- μ = Viscosity [Pa $\cdot$ s]
- V = Superficial velocity [m/s]

The superficial velocity is determined from the flow rate and cross-sectional area of the filter medium perpendicular to the flow directions [Brorsen and Larsen, 2007].

$$V = \frac{Q}{A} \tag{3.2}$$

- Q = Flow [m^3/s]
- A = Cross-sectional area [m^2]

Eq. 3.1 is valid only at low velocities [Lage et al., 1997]. During higher velocities the flow become effected by inertial forces and the relationship between the flow and pressure loss does not follow a simple linear relationship, which make Eq. 3.1 invalid [Trussell and Chang, 1999]. The flow reqime, where Eq. 3.1 applies, is called the Darcian flow regime [Trussell and Chang, 1999].

In the non-Darcy flow reqime, where the flow is still laminar, but dominated by inertial forces, the relationship between flow velocity and pressure loss typically follows a second order relationship.

Philipp Forcheimer proposed a two-term, second order model for predicting the $V-\Delta P$ relationship in this flow reqime as: [Trussell and Chang, 1999] [Zeng and Grigg, 2006].

$$-\frac{\Delta P}{L} = \frac{\mu}{k_a} V + \beta \rho V^2 \tag{3.3}$$

- β = Non-Darcy coefficient [-]
- ρ = Density of air [kg/m^3]

Equation 3.3 is essentially an extension of Eq. 3.1 with a second order velocity term. The first term of Eq. 3.3 is the linear Darcy Eq. 3.1, where the second part of the equation is the second order velocity term that account for the effects of inertial forces [Lage et al., 1997].

In the regime where the flow changes from being laminar to turbulent as well as in the fully turbulent regime is Eq. 3.3 also valid although the values of the coefficients k_a and C may be different from those found in the laminar regime [Lage et al., 1997].

3.2 Energy conversion during fluid flow in tubes

The pressure distribution is hydrostatic/aerostatic, if the flow lines are approximate parallel in each section of the biofilter. In this case the pressure-depth relation will be a straight line [Brorsen and Larsen, 2007]:

$$H_{liquid} \equiv (z + \frac{p}{\gamma}) + \frac{\alpha V^2}{2g} \tag{3.4}$$

- H = Energy level for liquid [m]
- z = Depth [m]
- p = Pressure [Pa]
- γ = Specific gravity [N/m^3]
- α = Constant set to 1.1 [-]
- V = Velocity [m/s]
- g = Gravitational acceleration [m/s^2]

The first part of the Eq. 3.4 is the hydrostatic pressure distribution and the second part is describing the fluid velocity.[Brorsen and Larsen, 2007]

For a conversion from meter into Pascal, has the gravitational acceleration and the density of air been multiplying with Eq. 3.4:

$$H_{air} \equiv P + \frac{\alpha V^2}{2g} \cdot g\rho \tag{3.5}$$

- H = Energy level for air [Pa]
- P = Pressure [Pa]
- g = Gravitational acceleration [m/s^2]
- ρ = Density of air [kg/m^3]

3.3 Pore flow characteristcs

3.3.1 Fluid flow across the entering of a pipe

When a fluid flow from a reservoir into a pipe, will the geometry of the entry result in a pressure loss [Munson et al., 2005]. A typical flow pattern for flow entering a pip through a square-edged entrance can be seen in Fig. 3.1.

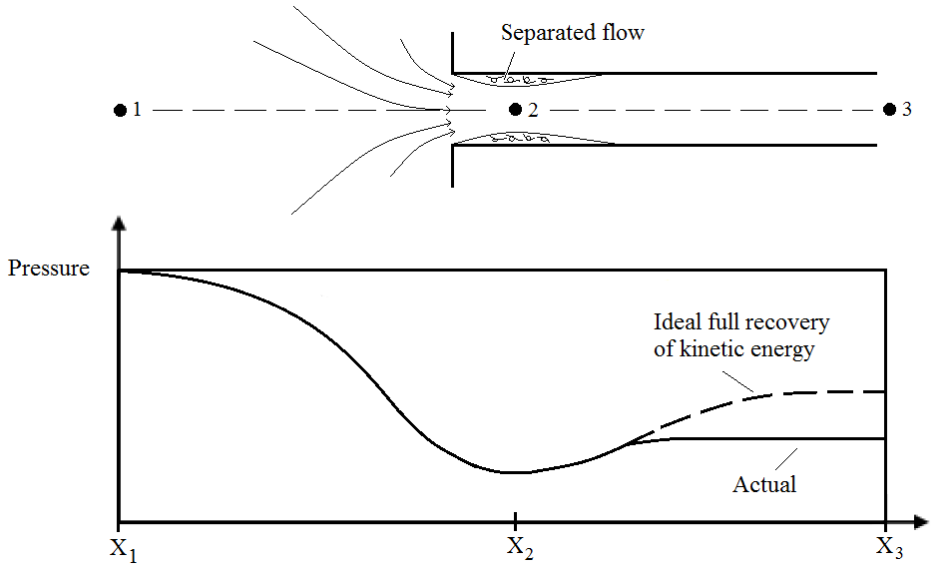

Figure 3.1: Flow pattern and pressure distribution for a sharp-edged entrance [Munson et al., 2005].

The square-edge of the entry will create a separated flow by the pipe wall (see section 2 on the first figure in Fig. 3.1), which will reduce the cross section area available for fluid transport and thereby speed up the fluid velocity [Munson et al., 2005].

In a system without losses, will there be an inverse relationship between velocity and pressure (see Eq. 3.5) to maintain the same energy level. Therefore does the acceleration of the fluid in section 2 give a pressure drop and furthermore will deceleration in section 3 result in a pressure increase. This pressure increase will be equal to the released energy from the deceleration. However as energy losses will be present in all systems with moving fluids, fluid energy level will decrease from section 1 - 3 [Munson et al., 2005].

3.3.2 Pore velocity within filter material

The pore velocity within the filter material is given as follows.

$$U = \frac{V}{\phi} \tag{3.6}$$

- U = Pore velocity [m/s]
- V = Superficial velocity [m/s]
- ϕ = Porosity [m^2 air/m^2 filter]

Variations in porosity and pore size will cause changes in the pore velocity and also in the pressure gradient [Brorsen and Larsen, 2007].

The porosity is found by:

$$\phi = 1 - \frac{P_B}{\rho} \tag{3.7}$$

- P_B = Bulk densicy [g/cm^3]
- ρ = Dencity [g/cm^3]

3.3.3 Flow in tubes with abrupt tube expansion in cross-sectional area

If the filter medium is regarded as a tube (or set of tubes), changes in porosity diameter (for instance in the filter outlet, where the porosity changes from filter material porosity to free air) can be analysed using the theory for flow in tubes. For instance in the inflow and outflow locations of the filter, the pores may be regarded as tubes that have an abrupt contraction or expansion.

For stationary flow in a pipe with an abrupt expansion (Fig. 3.2), intense eddies and turbulence in the expansion section, between the coulant and the eaux stagnantes fluid, will occur as illustrated in Fig. 3.2 [Brorsen and Larsen, 2007].

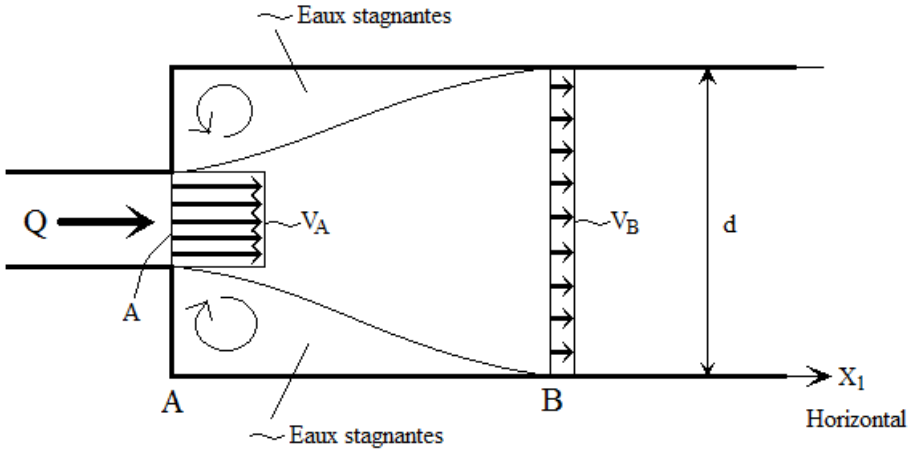

Figure 3.2: Illustration of flow conditions in a pipe with an abrupt expansion of cross sectional area. d is the diameter of the tube, Q is the flow and V is the velocity [Brorsen and Larsen, 2007].

When the flow lines diverge from location A (where the flow is uniform at high velocity) to location B (where the flow is again uniform, but with low velocity) the fluid pressure will increase in the flow direction [Brorsen and Larsen, 2007]. This increase in pressure can be estimated out from Eq. 3.8.

$$\Delta P = \frac{\rho Q^2}{B} \cdot \left(\frac{1}{A} - \frac{1}{B} \right) \tag{3.8}$$

- ΔP = The increased pressure after the filter [Pa]
- ρ = Density of air [kg/m^3]
- Q = Flow [m^3/s]
- A = Cross section area of the inlet tube [m^2]
- B = Cross section area of the outlet tube [m^2]

This theory is valid for flow in pipes, but may be applied to biofilters, which also have a narrowing at the entry of the filter (due to the presence of the material solids) and an expansion at the filter outlet.

Materials and methods 4

This chapter presents the materials and methods used and developed throughout this project.

4.1 Overview of experiments

Two sets of experiments were carried out, one under laboratory conditions and one under full-scale conditions.

Laboratory conditions

In the laboratory experiments four different types of Munters biofilters media and two different thicknesses were used. Pore sizes: 5 and 7 mm, and pore geometry with cross angles: 45^o & 45^o, 60^o & 30^o and 75^o & 45^o, have been examined.

To assess the pressure loss inside the biofilter material as a function of filter depth, measurements of pressure were taken before, inside and after the biofilters for a range of 9 different air velocities. An illustration of the experimental setup for the laboratory experiments is given in Fig. 4.1.

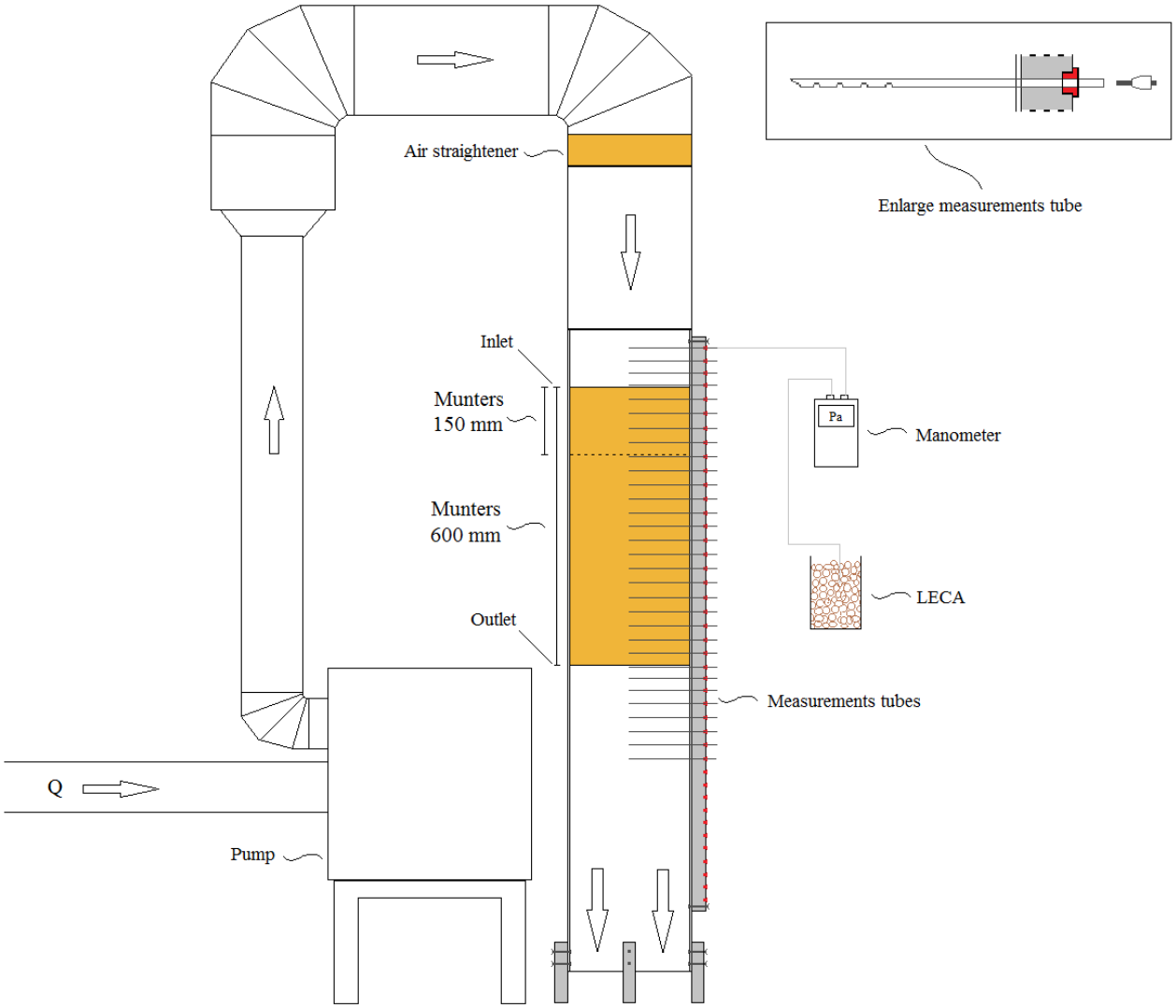

Figure 4.1: The setup of the 150 mm and 600 mm Munter biofilter, where the white arrows indicate the flow direction, Q. An enlarge measurements tube (upper right corner). The manometer and the reference point in LECA (to the right of the Munter filter).

Full-scale conditions

Full-scale experiments involving measurements of pressure loss and biomass content in an operating biofilter (with biomass present) were carried out at a test facility located at a pig farm on the northern part of the island Mors. This facility is operated by SKOV A/S and involves a series of consecutive biofilters as illustrated in Fig. 4.2

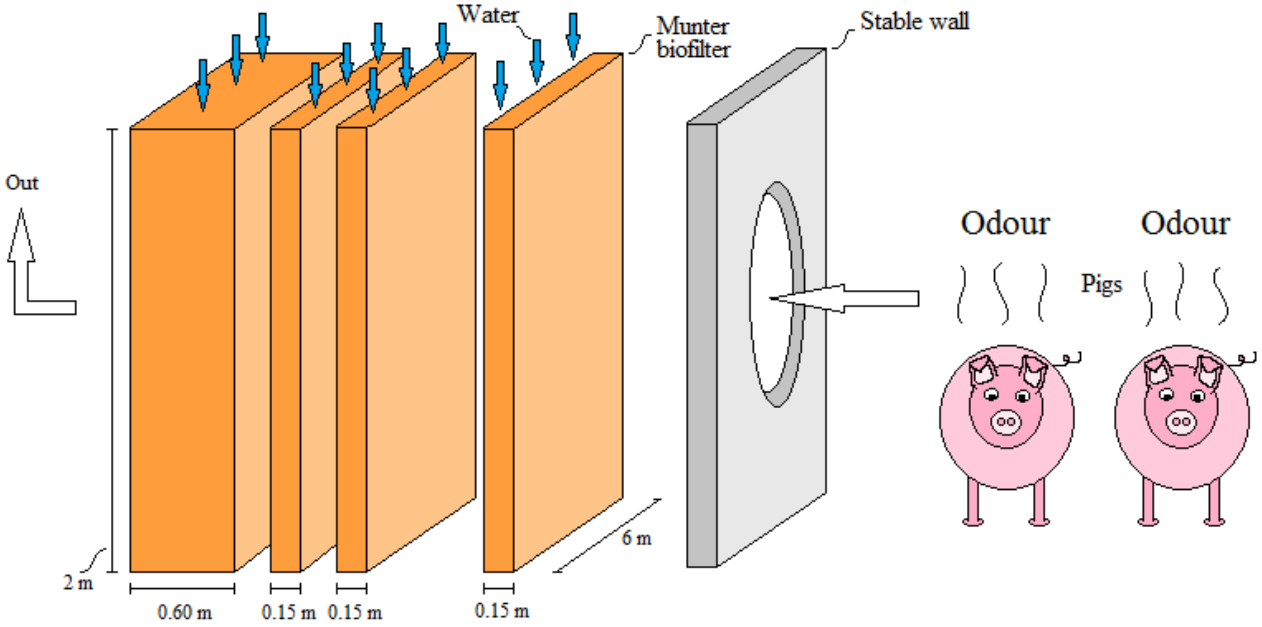

Figure 4.2: Illustration of the full-scale biofilter unit at northern Mors. The air from the pig shelter (right) was pumped into the experimental facility, illustrated with the grey wall and through the four biofilters, before the air was let outside.

The grey wall in Figure 4.2 have five large ventilation holes for transporting the air from the pig shelter and into the experimental facility, see Figure 4.3

Figure 4.3: The five ventilation holes to the right leading the polluted air from the pigsty and into the test facility and to the left the first biofilter.

4.2 Filter materials used

The biofilter material used in the laboratory experiments is produced by the Swedish company Munter AB and used for biofiltration by the Danish company SKOV A/S for cleaning contaminated air. The material is made of special impregnated cellulose fiber with rot prevention and water absorption capability [SKOV A/S, undated].

For the laboratory experiments four different biofilter materials, with different pore sizes, have been examined as described in Table 4.1.

Table 4.1: Biofilter characteristic.

Filter	Cross angle	Pore size [mm]	Bulk dencity, P_b [g/cm^3]	Porosity, ϕ [%]
A	45^o & 45^o	5	0.041	97.3
B	45^o & 45^o	7	0.026	98.3
C	60^o & 30^o	7	0.025	98.3
D	75^o & 45^o	7	0.023	98.5

The pores cross angles of the filters are given relative to the flow direction, see Fig. 4.4.

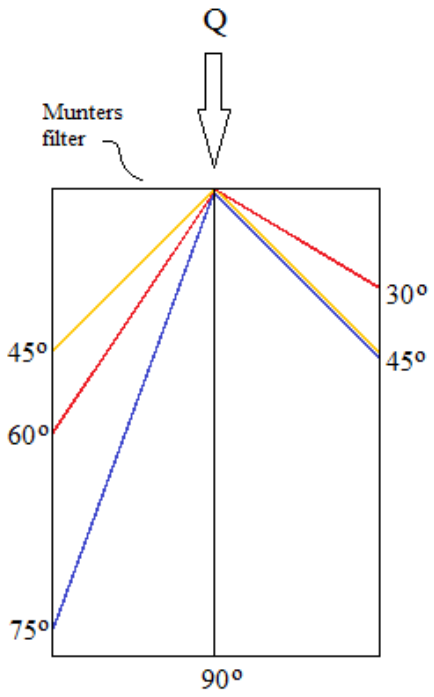

Figure 4.4: Illustration of the cross angles in the four Munters filters. Filter A and B (yellow), filter C (red) and filter D (blue). The black line illustrates a direct flow line across the filter.

The porosity in Table 4.1 is estimatede from Eg. 3.7, where the dencity of the Munters filter, made of cellulose, is set to 1.5 g/cm^3.

A illustrating picture of the filters A, B, C and D can be seen in Figure 4.5.

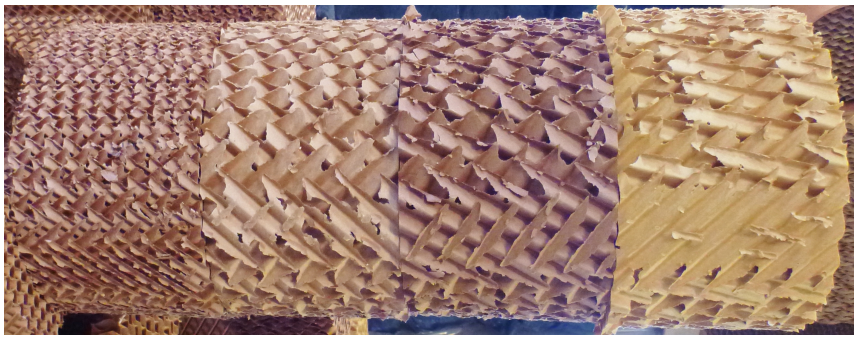

Figure 4.5: Four different Munter biofilters, with the thickness 150 mm. From the left is filter A, B and C and to the right is filter D shown.

All four filter materials were acquired in 150 mm thick sections and an additional 600 mm section was acquired for filter type D. At the test facility on Mors filter type D was also used in both 150 and 600 mm sections.

4.3 Experimental procedures

4.3.1 Laboratory scale measurements

Circular sections of the four biofilter media with a diameter of 250 mm (and 150 mm thickness) were prepared using a tube with a sharpened edge to cut the materials. An additional circular section with 600 mm thickness was prepared for material D. Each circular section was placed inside a 250 mm ventilation tube and connected to a CUBUFAN 160 EC ventilation pump (Jenk, Brøndby Denmark). An air straightener consisting of a 100 mm section of filter material was placed in front of the filter inlet to reduce air turbulence (Fig. 4.1).

Air flow through the Munters filter was measured continuously in the inlet to the pump using a VA400 thermal mass flow sensor, (CS instruments Tannheim Germany). Measurements were carried out for a range of selected air velocities as illustrated in Table 4.2.

Table 4.2: Flow velocities (Darcy velocities) used in the laboratory experiments.

Filter / Velocity [m/s]	0.44	0.75	1.06	1.37	1.67	1.99	2.30	2.62	2.75
A 15	+	+	+	+	+	+	+	+	-
B 15	-	+	+	+	+	+	+	+	-
C 15	-	-	+	+	+	+	+	+	+
D 15	-	-	+	+	+	+	+	+	+
D 60	+	+	+	+	+	+	+	+	-

Due to the minimum and maximum capacity of the pump it was not possible to achieve all velocities for all filter materials. All measurements were carried out in triplicate and duplicate circular sections of the filter materials were tested.

The differential pressure (between the filter and the atmosphere) was measured at 30 mm intervals before, inside and after the filter (Fig. 4.1), with a ALNOR AXD 560

manometer (Alnor, Ontario Canada). The differential pressure was measured using sharpened metal measurement tubes (inner and outer diameter were 2 and 3 mm respectively), that were penetrated through the Munters filter from the side of the ventilation tube, such the end point (where the pressure is to be measured) of the measurement tubes are located in the centre of the ventilation tube (125 mm from the inside wall).

The 150 mm and 600 mm biofilter sections were located in the ventilation tube such that their inlet was in the same position (Fig. 4.1). The reference point of the manometer (for measuring the differential pressure) was located outside the filter in a glass jar containing LECA, to reduce the pressure fluctuations caused by air movement in the laboratory.

Differential pressure was measured in three locations before the filter inlet and seven after the filter outlet. The three measurements, before the filter inlet, were taken to obtain a good average value of the inlet differential pressure and seven measurements, after the filter outlet, were taken to capture pressure variations after the filter outlet. The reason is that the system regains pressure after the filter exit. One pressure measurement was taken exactly in the filter inlet and one in the filter outlet to identify the pressure loss over the filter material itself. An additional four measurement locations were used for the 150 mm Munter filter and 19 measurement locations for the 600 mm filter were used to determine pressure variations inside the filter materials.

Additional measurements of the total pressure drop across the D 15 cm filter was made using the setup in Fig. 4.6.

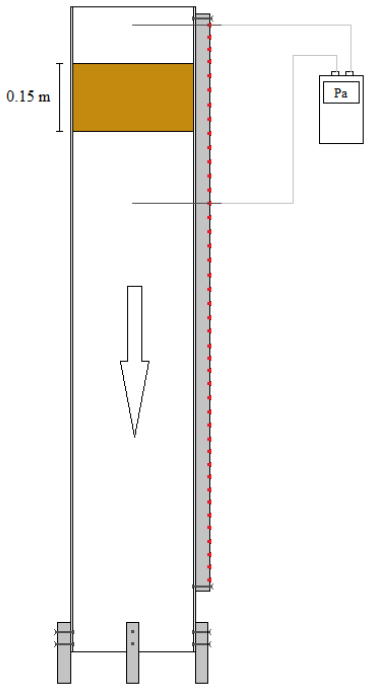

Figure 4.6: Experimaental setup of the 0.15 m Munter filter type D. The manometer measuring the total pressure drop over the filter, where the reference point is located 0.15 m after the 0.15 m filter.

This experimental setup was made for comparison with the data measured at the test facillity on Mors. Three velocities were used in these measurements: 0.2, 0.3 and 0.4 m/s, which covers the measured velocity at the test facility of: 0.29 m/s.

4.3.2 Development and test of the pressure tubes

Part of the measurement program included development and design of the pressure measurement tubes.

Two possible tube designs were tested. One design only had a hole at the end point (where it was cut at an angle), and the other had in addition the hole at the end and also for extra holes along the side of the tube (see illustration in Fig. 4.7).

Figure 4.7: The measurement tube with one hole (left) and a tube with four extra holes (right).

The extra holes in the left measurement tube design were made, because of the flow velocity and thus, the pressure varies as a function of location within single pores. Therefore

one hole in the measurement tubes may not be enough to get a representative measurement, because the tip can be located differently within each filter pore for the different depths resulting in increased variability in the measured pressures. The four extra holes will therefore average out this variation within the same filter depth, such that a more accurate measurement of the average pressure at that depth will be achieved.

To illustrate the effect of the two designs, the pressure variation inside a 600 mm filter section is plotted as a function of depth in Fig. 4.8 for each of the designs.

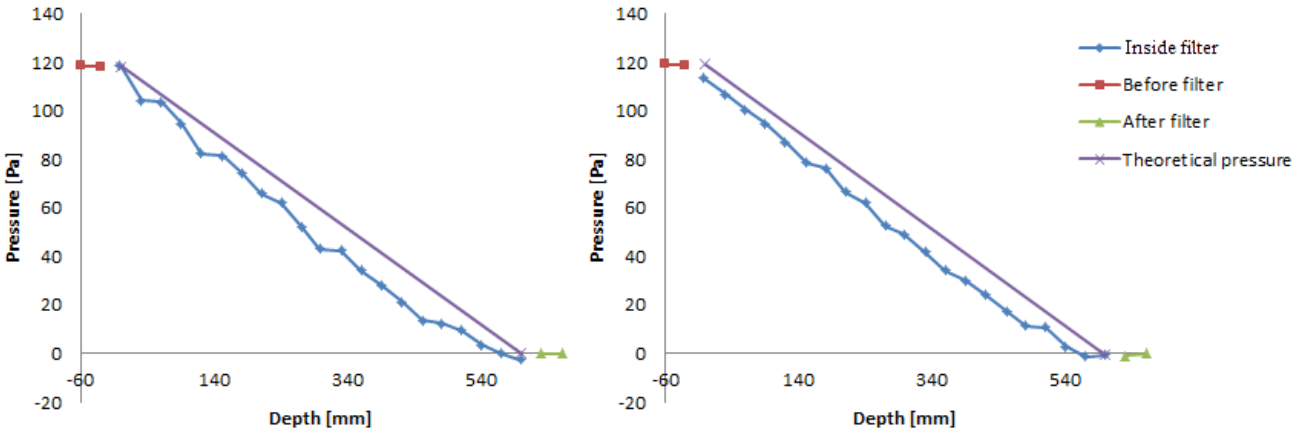

Figure 4.8: The two graphs show measurements before a 600 mm D filter (red), two measurements after the filter (green), 21 measurements are inside the Munter filter (blue), where the measurement tubes are without extra holes (right) and with extra holes (left), theoretical pressure drop (purple). The measured velocity is approx. 2.60 m/s.

Figure 4.8 show that the measurements with extra holes in the measurement tubes have a more even progress of the pressure drop as a function of depth and this design was therefore used in all subsequent measurements.

It was further tested if leaving measurement tubes open to the atmosphere would have an influence on the measured pressures. Measurements were carried out under conditions where the measurement tubes were not plugged and conditions where each measurement tube was plugged to prevent direct connection to the atmosphere. A sketch of the two possibilities is given in Fig. 4.9

Figure 4.9: The measurement tube without a plug (left) and with a plug (right).

The effect of the two approaches is seen in Fig. 4.10, where the last seven pressure measurements, taken after the filter, are plotted as a function of depth.

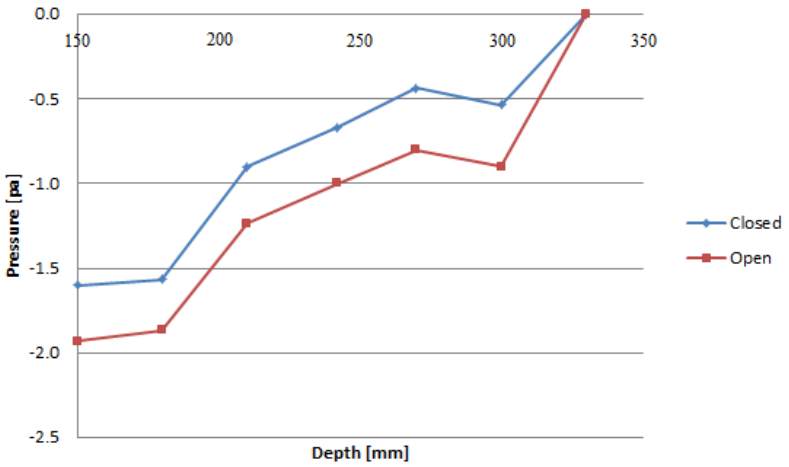

Figure 4.10: The pressure as a function of depth, where seven measurements with closed measurement tubes (blue) and with open tubes (red). The end of the 150 mm filter is at x = 150.

Figure 4.10 clearly shows a smaller pressure loss with closed measurement tubes, compared with the open tubes and closed tubes were therefore used in all subsequent measurements.

4.4 Full scale measurements

At the test facility on Mors (Fig. 4.2), the air was pumped through the four biofilters units at a flow of approx. 12,500 m^3/h (0.29 m/s) on the measuring day, before exiting the facility.

The four biofilter sections were irrigated with water from a system placed above the filters and the irrigation was running in the sequence of 70 sec for every 100 sec. The front of the first biofilter unit was observed to be drier than the backside, and the filters were also not equally wet in all locations.

The biofilters had not been washed for seven month, and the biofilm on the first biofilter unit was therefore very thick, see illustration on Fig. 4.11.

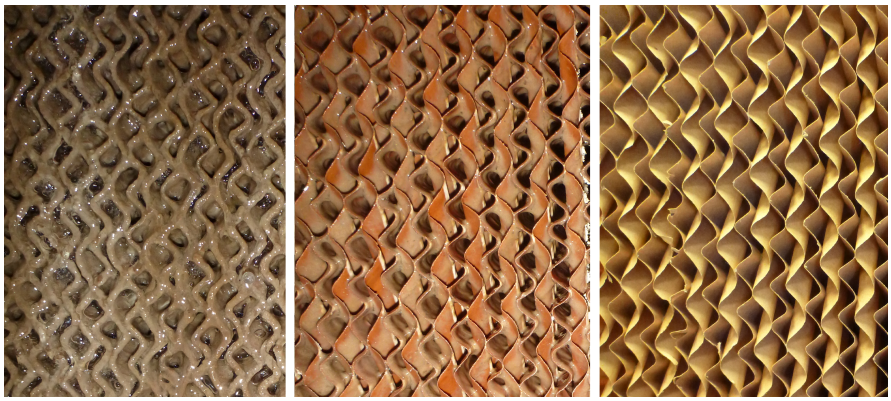

Figure 4.11: The front of the first filter unit (right), back of the filter (centre) and a clean filter (left).

The biofilm on the other filter sections was not as developed and measurements of pressure drop and biomass were therefore only taken from the first biofilter section.

The total pressure drop across the first biofilter section were taken in three locations using a thin metal tube connected to the manometer, see Fig. 4.12.

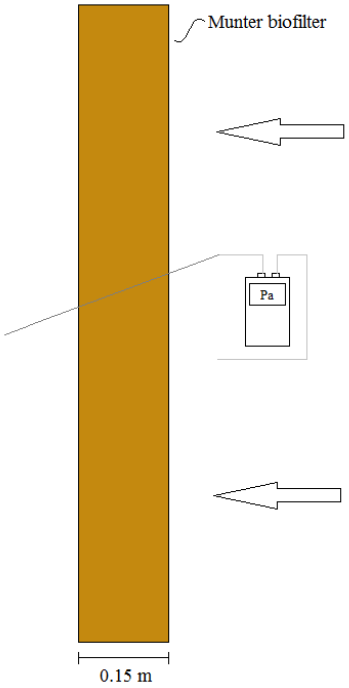

Figure 4.12: Full scall setup at the test facility at Mors. The manometer measuring the total pressure over the 0.15 m thick biofilter.

The pressure measurement locations were between location 1 and 2, one at location 3 and the last in between location 4 and 5 (see Fig. 4.13). All measurements were carried out in triplicate.

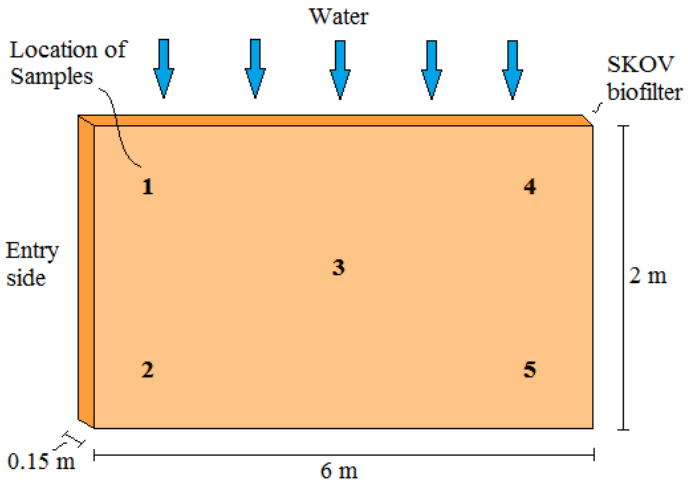

Figure 4.13: Illustrate the five sample locations on the Munter biofilter. The entry side into the filter is located to the left. The dimensions: 2 x 6 x 0.15 m

Three samples of the biofilm were taken at five different locations on the front and back of the first biofilter unit. These are indicated on Fig. 4.13.

The biofilm samples were collected using a small scraping device developed especially for this purpose, see Fig. 4.14.

Figure 4.14: The scraper scraping a clean Munter filter of type D. The two marked black lines on the scraper indicate 1 cm each. The black rubber on the scraper is 1.1 cm in width.

At each sample location the pore wall was scraped three times at the same angle, to make sure that all the biofilm was collected.

The three biomass samples from each of the five locations on both front and back of the filter were weighed right after sampling and then transported to the laboratory. Here they were placed in an oven at 105 ^{o}C to dry for 18 hours. After the 18 hours were the samples taken out of the oven and weighed to determinate the dry matter content.

Results and discussion 5

This chapter presents the results and discussion of the laboratory and full-scale experiments.

5.1 Pressure loss and pressure gradients across the filter media

The $V-\Delta P/L$ relationships measured for the four biofilter media during the laboratory experiments were observed to follow a second order equation in agreement with Eq. 3.3 (Fig. 5.1). Althought Eg. 3.3 predicts that the $V-\Delta P$ relationship is the same regardless of filter medium thickness, were not the case for the experimental observations for filter material D, where two thicknesses were available (Fig. 5.1).

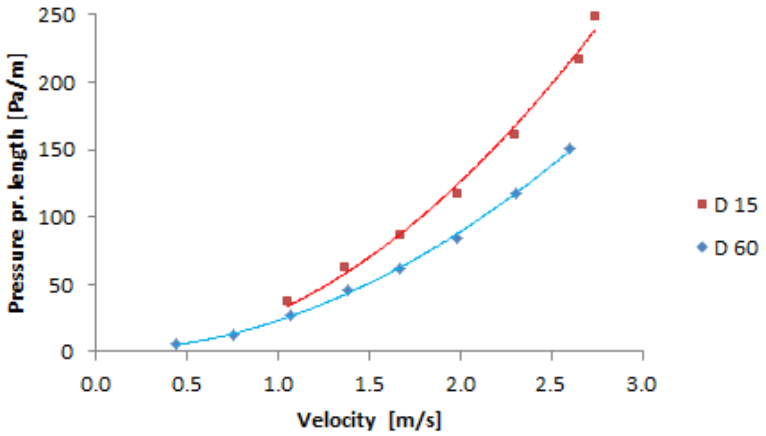

Figure 5.1: The pressure pr. length as a function of velocity. Filter type D 15 cm (red) and D 60 cm (blue).

Figure 5.1 show that the apparent pressure gradient across a 15 cm biofilter unit is higher than the apparent pressure gradient across a 60 cm biofilter units although in theory (assuming a linearly decreasing pressure across the filter unit) they should be the same. This clearly indicate that there are pressure losses that are unaccounted for by Eg. 3.3.

Figure 5.2 shows the differential pressure as a function of depth for the 15 and 60 D-filter sections. Similar observations were also done for the A, B, and C filter sections.

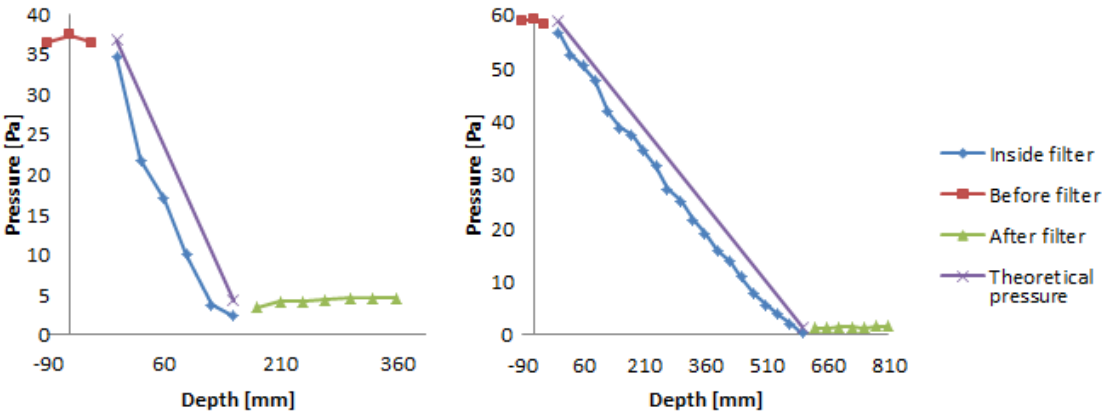

Figure 5.2: The two plots show filter D 15 cm (left) and D 60 cm (right) as a function of depth. Three measurements before the filter (red), 6 and 21 measurements through the Munter filter for 15 cm and 60 cm respectively (blue) and the theoretical pressure (purple). The velocity for both graphs is 2.65 m/s.

Figure 5.2 show that the variation in pressure as a function of depth in the filter column (indicated by the blue points) don't follow the theoretical pressure variation (indicated by the purple linear line) based on the Darcy or Forcheimers theory described in section 3.1. Although the pressure gradient inside the filter material appears to be linear for most of the filter depths, does the behavior in pressure near the in- and outlet not follow the Darcy or Forcheimer theory.

Figure 5.2 further shows that the pressure loss is higher near the inlet, then decreases and becomes constant, when inside the filter and then decreases again near the outlet. Furthermore can an increas in the pressure after the filter outlet be observed.

A closeup of the pressure variation near the filter outlet for the 15 cm D-filter material for different velocities is shown in Fig. 5.3. From this plot it is very clear that the pressure increases after the filter outlet and the increase is greater for higher velocities. Similar observations were done for the other filter materials and air velocities.

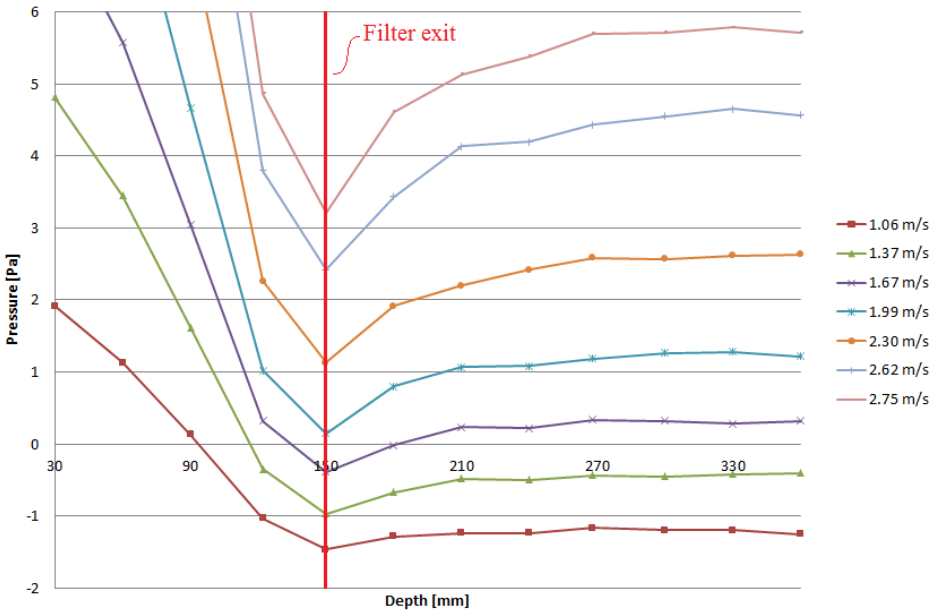

Figure 5.3: The measured pressure before the exit of D 15 filter medium and seven measurement after the filter, where the red line indicate the filter exit.

The small increase in the pressure after the filter outlet corresponds with the theory for flow in tube with abrupt increase in cross sectional area.

Inside the filter material the effective cross sectional area is smaller than after the filter outlet, because part of the space inside the filter is taken up by the medium itself. Another part of the porosity, although it is air-filled, does not take part in the flow as the air here is stagnant. This is for instance air in small corners or behind edges, where there may be circulating currents or turbulence, but no convective air flow.

The effective porosity of the filter media were estimated using Eq. 3.8, for each filter medium and velocity, where the point "A" in Eq. 3.8, is located at the transition from filter material to empty column (red line in Fig. 5.3) and "B", when the pressure is at steady state after the filter.

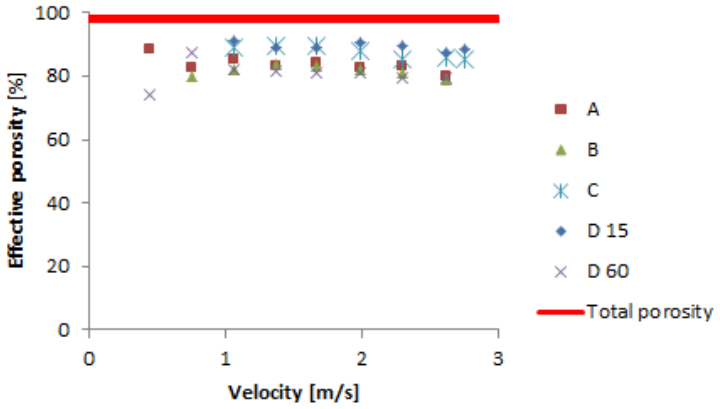

Figure 5.4: The effective porosity as a function of velocity within the four different filters A, B, C and D, and the total porosity (red line).

Figure 5.3 show the effective porosity, for the different filters, are all lower than the total porosity (see Fig. 4.1). The figure also shows that the effective porosities are generally independent of the velocity, within the range of velocities investigated.

The pore velocity can be estimated from the effective porosity using Eq. 3.6. The effective velocity and the pressure gradient can further be used in Eq. 3.5 to estimate the energy level before, inside and after each filter unit.

As the energy level depends on both pore velocity and pressure, it can then be used to identify and explain variations in the pressure level.

The energy levels as a function of filter depth estimated using Eq. 3.5 for filter materials D 15 and D 60 are shown in Figure 5.5.

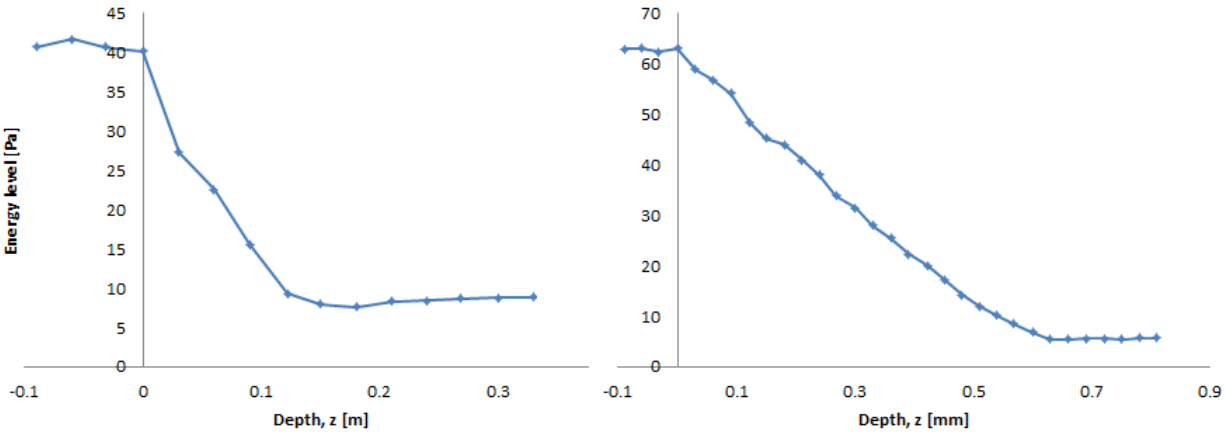

Figure 5.5: The energy level as a function of depth for filter D 15 (left) and D 60 (right). The velocity is 2.65 m/s.

Similar observations were also made for the other filter materials and velocities. Figure 5.5 shows that the energy level in some locations seems to increase a bit. This is not physically possible and is a result of small uncertainties in the measurements.

5.1.1 Modelling energy turnover and energy level

The energy level at any location inside the column, containing the filter unit, can be modelled as:

$$E(z) = E_{in} - F_L - T_{L \cdot In} - T_{L \cdot Out} \tag{5.1}$$

- z = Filter depth [m]
- E_{in} = Starting calculated energy level
- F_L = Filter loss
- $T_{L \cdot In}$ = Transition loss at the entrance
- $T_{L \cdot Out}$ = Transition loss at the exit

E_{in} is the energy level at a selected reference location (in this study selected before the inlet of each filter unit. The filter loss F_L is modelled as: $F_L = K_f \cdot z$, following the theory of Darcy and Forcheimer. The parameter K_f is a constant that depends on the permeability of the filter material. The transition losses at the entrance and exit ($T_{L \cdot In}$ and $T_{L \cdot Out}$ respectively) are not assumed instantaneous at the inlet and outlet location, instead the losses are assumed distributed over a certain distance of the filter near the inlet and outlet. The distribution of the transition losses is assumed to follow a normal distribution function, which means that the transition losses can be modelled as:

$$T_{L \cdot In}: \qquad -\frac{K_{in}}{2}\left(1 + erf\left[\frac{z - z_{in}}{\sqrt{2\sigma_{in}^2}}\right]\right) \tag{5.2}$$

- z = Filter depth [m]
- erf = Error function [m]
- F_L = Constant of the filter slope [-]
- K_{in} = Constant of the transition loss, which describe the height at the entrance [-]
- σ_{in} = Constant of the transition loss, which describe the wide at the entrance [-]

$$T_{L \cdot Out}: \qquad -\frac{K_{out}}{2}\left(1 + erf\left[\frac{z - z_{out}}{\sqrt{2\sigma_{out}^2}}\right]\right) \tag{5.3}$$

- z = Filter depth [m]
- erf = Error function [m]
- K_{out} = Constant of the transition loss, which describe the height at the exit [-]
- σ_{out} = Constant of the transition loss, which describe the wide at the exit [-]

Equations 5.2-5.3 were fitted to the energy level data based on the pressure and velocity measurements (as those in Fig. 5.5) by optimizing the values of K_f, K_{in}, σ_{in} $\geq$0.001, K_{out} and σ_{out} $\geq$0.001, while minimizing the sum of squared deviations between modelled and measured energy data, see Appendix A for all the measured and modelled parameters for each filter unit and velocity.

As the effective porosity is unknown at filter in- and outlet, H_{air} in Eq.(3.5) cannot be correctly estimated for these locations. These locations (0 and 150 mm for 15 cm filters and 0, 30, 568 and 600 mm for 60 cm filters) have therefore been excluded from the fitting of Eq. (5.1).

The measured and modelled energy levels for the two filter materials D 15 and D 60 can be viewed in Fig. 5.6.

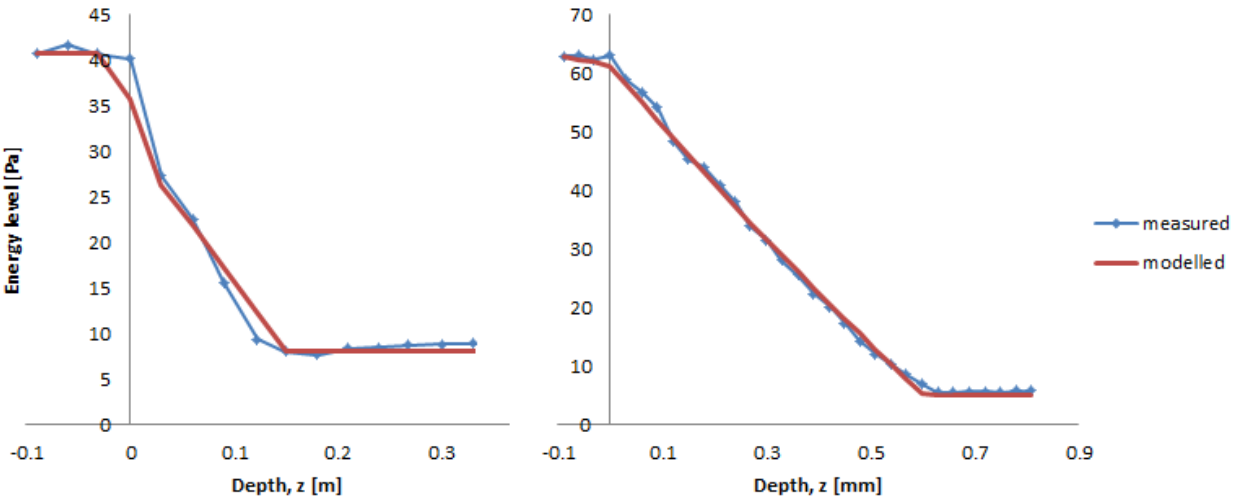

Figure 5.6: The modelled energy level as a function of depth for filter D 15 (left) and D 60 (right). The measured and modelled energy level is respectively blue and red. The velocity is 2.65 m/s.

Figure 5.6 show a close fit between the modelled and measured energy level for filter D 60 (RMSE: 0.82), which indicate that a good agreement between measurements and theory. The fit for filter D 15, is less accurate (RMSE: 1.09), which could be caused by the smaller amount of measurements across the filter. For the remaining filters A, B and C a close fits for the same velocity were obtained (RMSE: 0.79, 0.83, 0.94 respectively, see Appendix A). If a comparison of RMSE % of ΔP, see Appendix A, is made between all the filter units does A have the best fit (0.86 %), then D60, B, C and at last D15 (0.98 %, 1.23 %, 1.64 % and 2.96 % respectively).

5.1.2 Comparison between the four filters

The modelled energy level as a function of depth in the four filter types, with the velocity 2.65 m/s, can be viewed in Figure 5.7.

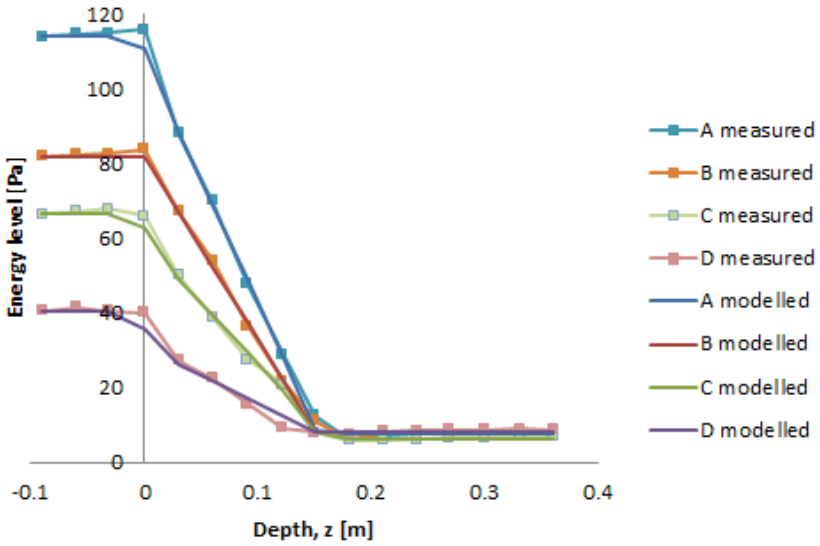

Figure 5.7: The measured and modelled energy level as a function of depth. Filter A (blue), B (red), C (green) and D (purple). The velocity is 2.65 m/s.

Figure 5.7 show that the energy level variation as a function of filter depth for filters A, C and D, is not linear inside the filters, while it is linear for filter B. The graphs differed the most near the entry and exit of the filters, which could be assumed to be due to the minor losses.

Furthermore the highest energy level is found in the smallest pore size (filter A). This is because a smaller cross section area will cause an increase in the pressure gradient and an increase in the velocity and therefore a higher energy level.

The inlet energy level decreases in the order: A, B, C and D. This corresponds to the cross angles of the filter material. Filter D for example has a large cross angle, 75^o & 45^o (Table 4.1 on page 14), perpendicular to the flow direction, resulting in a smaller filter resistance and therefore a lower energy level. Filter B and C have cross angles of 45^o & 45^o and 60^o & 30^o respectively, which are the second and third largest cross angles after filter D and are therefore resulting in the second and third lowest energy level respectively.

A comparison between the total pressure drops over each of the four 15 cm filter units as a function of velocity is given in Fig. 5.8.

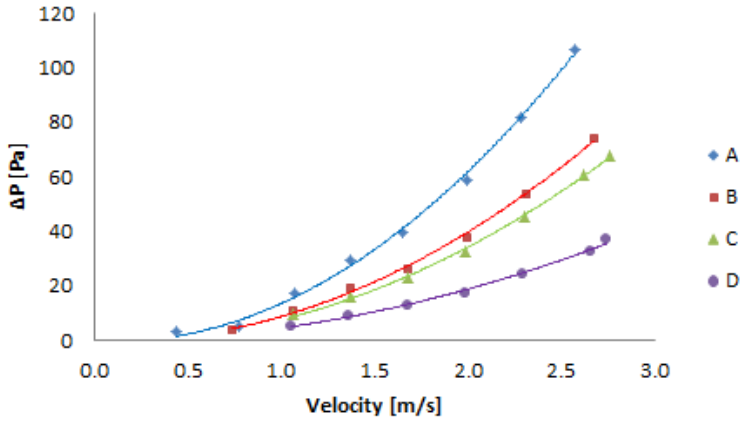

Figure 5.8: The pressure gradient as a function of velocity for the four 15 cm filters, A (blue), B (red), C (green) and D (purple).

Figure 5.8 show that all four relationships follow a quadratic equation in agreement with the Forcheimer theory (Eq. 3.3). This graph also shows that the smaller the pore size and cross angles of the filter materials, the higher the total pressure loss.

Filter B and C are very similar with respect to total pressure loss, which could be caused by the similarity in pore size and cross angles within these filters.

Filter D has the smallest ΔP, which correspond with the large cross angle: 75^o & 45^o and pore size: 7 mm.

A comparison of the minor losses, represented by the constant K_{in}, (Eq. 5.2), over each filterunit, as a function of velocity is shown in Fig. 5.9.

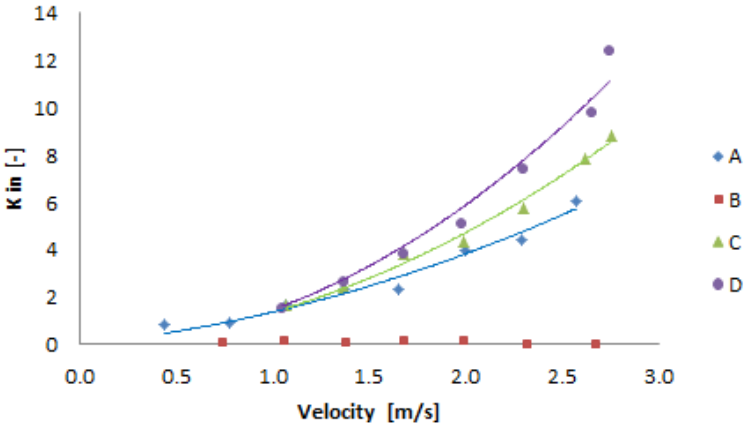

Figure 5.9: The constant K_{in} as a function of velocity for the four 15 cm filters, A (blue), B (red), C (green) and D (purpel).

Figure 5.9 show that with the exception of filter B, the constant K_{in} also follows a second order relationship with velocity and thus, could be described by the Forcheimer

theory.

K_{in} (see Fig. 5.9) is further observed to increase at increasing pore size. However as the true distribution of minor losses over the entrance region is unknown this phenomena could be caused by the enclosed assumptions of the energy loss in Eq. (5.1).

K_{out} on the other hand does not give a precise response, compared with K_{in} and have therefore not been used further.

5.2 The results from the full scale measurements on the test facility on Mors

The relationship between the biofilm mass per filter pore on the front and back of the first biofilter section of the test facility, can be seen in Fig. 5.10.

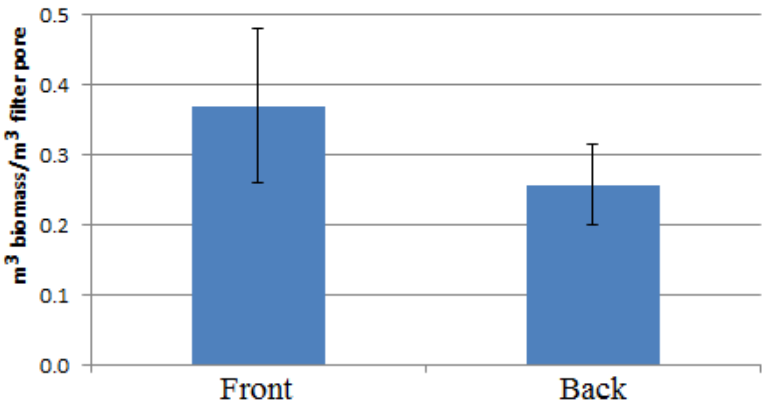

Figure 5.10: The biofilm mass per filter pore on the front (left) and back (right) of the first biofilter. The standard deviations are shown in each of the two columns.

Figure 5.10 show a more develop biofilm on the front (37.0 % of the pore) of the first biofilter compared with the back (25.8 % of the pore). This corresponds with the research made by Morgan-Sagastume et al. [2001], who have found that higher concentration of biomass are developed in the inlet of the filter compared with the outlet of the filter.

The dry matter contents were in general lower on the front (4.7 % in average) then on the back (6.9 % in average).

The pressure drop over the 15 cm active biofilter was measured to 3.64 Pa, where under laboratory experiments it was measured to 0.22 Pa. It can therefore be assumed that the total pressure gradient will be reduced significantly, when a developed biofilm is present, which also correspond well with the research of Morgan-Sagastume et al. [2001], who have found that the key factor for an increase in the pressure drop is caused by bed clogging due to biomass growth and therefore the highest pressure drop will occur in sections, where high biomass levels are present.

Conclusion 6

Pressure gradients (ΔP) across four commercial (Munters AB) biofilter materials with different pore sizes and pore orientations were measured over a range of different velocities.

ΔP were observed to increase for increasing velocity, decreasing pore size and increasing flow bending caused by different angles of the flow conducting pores in the media.

The $V - \Delta P/L$ relationships measured for the four biofilter media, A, B, C and D (15 and 60 cm) were observed to follow a second order relationship in agreement with the Forcheimer equation. The $V - \Delta P$ relationship was further observed to vary with filter medium thickness despite the fact that the commonly used theory for flow in porous media predict that it should be independent of filter thickness.
This variation is caused by what is termed minor losses of energy over the entry and exit of the filter media.

In addition an increase in pressure downstream the filter outlet was observed together with an increase in velocity, which correspond with the theory for flow in tubes with an expansion of the cross sectional area.

The effective porosity, for the four filter media, were found to be smaller than the total porosity. The effective porosities were generally observed to be independent of the velocity, within the range of velocities investigated.

The measured energy levels for each filter and velocity were successfully modelled, using a model based on the theory for energy level in moving fluids under aerostatic pressure distributions.

Based on the modelled energy level was it found that the bigger the pore size the larger the minor losses over the entry of the filter medium. This indicates that the assumption of a normal distribution function for the minor losses are not totally correct and further improvements of the model and the fitting procedure are necessary.

On site measurements, in a full scale biofilter connected to a pig stable, were performed to investigate the impact of biofilm on biofilter pressure drop.

Presence of biofilm was observed to increase biofilter pressure drop significantly. It was also observed that the biofilm thickness was largest at the filter inlet and decreased with filter depth.

In conclusion this project shows that there exist minor pressure and energy losses over the inlet and outlet of biofilter media (something that has not previously been documented) and that it is possible to model these losses.

In addition does the results obtained in this study indicate that when designing a biofilter for cleaning polluted air, the pore size, pore orientation and biofilm thickness should be taken into account for minimising the pressure drop across the biofilter, which will further lower the operational costs.

Future perspective 7

Throughout this report the minor energy losses over the entry and exit of the Munters filter units have been presented and discussed including the relationship between the pressure variation and minor losses. It is however, still unknown how these losses depend on filter material characteristics such as:

- The density and distribution of biomass within an active biofilter.
- The media characteristic such as medium cross angles and pore size.

Also the exact location, where the minor losses actually take place, is still unknown.

Another point of view, which will give a better understanding of the minor losses over the entry and exit of the filter, will be a more detailed velocity profil over the pores at each depth. These measurements will enable more accurate modelling of the energy turnover, because the energy level can be determined with greater detail as a function of depth and therefore no assumption of how the velocity behaves across the filter inlet and outlet have to be made, but exact measurements can be used instead.

It could also be interesting to link parameters like the media characteristics with the flow velocity to enable prediction of the pressure drop for a given medium at a given velocity, without having to resort to assumptions.

Bibliography

Brorsen and Larsen, **2007**. M. Brorsen and T. Larsen. *Lærebog i Hydraulik*. 1. udgave, 3. oplag. Aalborg Universitetsforlag, 2007. ISBN: 978-87-7307-691-0.

Chin and Hoff, **2009**. L. Chin and S. J. Hoff. *Mitigating Odors from Agricultural Facilities: A review of Literature Concerning Biofilters*. Applied Engineering in Agriculture, 25(5), 751–766, 2009.

Dansk Landbrugsrådgivning, **undated**. Dansk Landbrugsrådgivning. *Lugt - Problemer og Løsninger*. URL: `http://www.landbrugsinfo.dk/ledelse/Strategi/Miljoestrategi/Filer/140818ms_Lugt_09.doc`, undated. Downloaded: 14-02-2012.

Delhoménie, Bibeau, Gendron, Brzezinski, and Heitz, **2003**. M. C. Delhoménie, L. Bibeau, J. Gendron, R. Brzezinski, and M. Heitz. *A study of clogging in a biofilter treating toluene vapors*. Chemical Engineering Journal 94, pages 211–222, 2003.

Kim and Deshusses, **2008**. S. Kim and M. A. Deshusses. *Determination of mass transfer coefficients for packing materials used in biofilters and biotrickling filters for air pollution control*. Chemical Engineering Science, 63, 841 – 855, 2008.

Lage, Antohe, and Nield, **1997**. J. L Lage, B. V. Antohe, and D. A. Nield. *Two Types of Nonlinear Pressure-Drop Versus Flow-Rate Relation Observed for Saturated Porous Media*. Journal of Fluids Engineering, 119, 700–706, 1997.

Lyngbye, Hansen, Riis, Jensen, and Sørensen, **undated**. M. Lyngbye, M.J. Hansen, A.L. Riis, T.L. Jensen, and G. Sørensen. *1000 Olfactometry Analyses and 100 TD-GC/MS Analyses to Evaluate Methods for Reducing Odour from Finishing Units in Denmark*. Agricultural Air Quality, page 138–152, undated.

Macdonald, El-Sayed, Mow, and Dullien, **1979**. I. F. Macdonald, M. S. El-Sayed, K. Mow, and F. A. L. Dullien. *Review: Flow through Porous Media - the Ergun Equation Revisited*. American Chemical Society, 18, No, 18, 199 – 208, 1979.

Minelgaite, Andreasen, and Poulsen, **2012**. G. Minelgaite, R. R. Andreasen, and T. G. Poulsen. *Pressure Gradient through Porous Biofilter Material. Initial Pressure Drop at the Front End of the Filter media*. Department of Biotechnology, Chemistry and Environmental Engineering, pages 1–15, 2012.

Morgan-Sagastume, Sleep, and Allen, **2001**. F. Morgan-Sagastume, B. E. Sleep, and D. G. Allen. *Effects of Biomass Growth on Gas Pressure Drop in Biofilters*. Journal of Enviromental Engineering, page 388 – 396, 2001.

Munson, Young, and Okiishi, **2005**. B. R. Munson, D. F. Young, and T. H. Okiishi. *Fundamentals of Fluid Mechanics*. Wiley, 2005. ISBN-13: 978-0471675822.

O'Neill, Stewart, and Phillips, **1992**. D. H. O'Neill, I. W. Stewart, and V. R. Phillips. *A Review of the Control of Odour Nuisance from Livestock Buildings: Part 2, The Costs of Odour Abatement Systems as Predicted from Ventilation Requirements.* The Silsoe Research Institute, 51, 157–165, 1992.

Riis, Hansen, and Jensen, **2006**. B. L. Riis, A. G. Hansen, and T. L. Jensen. *Luftrensning til stalde. Videreudvikling af biofiltre til eksisterende staldanlæg med akutte lugtproblemer. – pilottest ved svinestald.* Miljøministeriet, (31), 2006.

Schiffman, Miller, Suggs, and Graham, **1994**. S. S. Schiffman, E. A. Saltely Miller, M. S. Suggs, and B. G. Graham. *The Effect of Environmental Odors Emanating From Commercial Swine Operations on the Mood of Nearby Residents.* Pergamon, pages 369–375, 1994.

Schwarz, Devinny, and Tsotsis, **2001**. B. C. E. Schwarz, J. S. Devinny, and T. T. Tsotsis. *A bioflter network model - importance of the pore structure and other large-scale heterogeneities.* Pergamon, 56, 475–483, 2001.

Shareefdeen and Singh, **2005**. Z. Shareefdeen and A. Singh. *Biofiltration for Odor and Air Pollution Control.* Springer, 2005. ISBN: 3-540-23312-1.

SKOV A/S, **undated**. SKOV A/S. *Luftrensning.* URL: `http://www.skov.com/DA/Components/luftrensning/Pages/Default.aspx`, undated. Downloaded: 14-02-2012.

Trussell and Chang, **1999**. R. R. Trussell and M. Chang. *Review of flow through porous media as applied to head loss in water filters.* Journal of Environmental Engineering, pages 998–1006, 1999.

Zeng and Grigg, **2006**. Z. Zeng and R. Grigg. *A Criterion for Non-Darcy Flow in Porous Media.* Springer, 63, 57–69, 2006.

Filter characteristic A

The following tables show the four filter: A, B, C, D15 and D60 characteristic. The different parameter: ΔP, $\phi_{effective}$, K_{in}, K_{out}, F_L, σ_{in}, σ_{out}, E_{in}, RMSE and RMSE % of ΔP, which have been measured and modelled are shown together with different volocities, V, measured for each filter.

Table A.1: Filter A 15 cm. Cross angles: 45^o & 45^o. Pore size: 5 mm. Total porosity: 97.3 %

V [m/s]	ΔP [Pa]	$\phi_{effective}$ [%]	K_{in}	K_{out}	F_L [Pa/m]	σ_{in}	σ_{out}	E_{in} [Pa]	RMSE	RMSE/ΔP [%]
0.44	3.7	88.6	0.8	0.038	18.4	0.20	0.001	2.5	0.03	0.85
0.77	5.4	82.6	0.9	0.030	41.4	0.29	0.001	6.5	0.08	1.50
1.07	17.6	85.5	1.7	0.002	101.8	0.55	0.001	17.5	0.15	0.84
1.37	29.7	83.4	2.3	0.006	177.3	0.74	0.001	30.5	0.18	0.60
1.65	39.9	84.1	2.3	0.006	239.9	1.06	0.001	41.3	0.38	0.95
1.99	59.2	82.7	4.0	0.002	354.5	1.69	0.001	62.3	0.42	0.71
2.29	81.6	82.9	4.4	0.006	497.5	1.96	0.001	86.5	0.57	0.70
2.57	107.0	80.1	6.0	0.005	653.7	2.45	0.001	114.1	0.79	0.74
									Average:	0.86 %

Table A.2: Filter B 15 cm. Cross angles: 45^o & 45^o. Pore size: 7 mm. Total porosity: 98.3 %

V [m/s]	ΔP [Pa]	$\phi_{effective}$ [%]	K_{in}	K_{out}	F_L [Pa/m]	σ_{in}	σ_{out}	E_{in} [Pa]	RMSE	RMSE/ΔP [%]
0.73	4.3	80.1	0.12	0.002	27.7	0	0.001	2.9	0.05	1.26
1.06	11.2	82.0	0.15	0.003	72.5	0	20.6	10.5	0.15	1.31
1.37	19.2	83.7	0.13	0.003	125.9	0	20.6	19.5	0.24	1.25
1.67	26.7	83.2	0.16	0.003	175.0	0	20.6	28.0	0.35	1.31
1.99	38.0	81.8	0.16	0.002	250.0	0	20.6	40.9	0.46	1.20
2.31	53.8	81.1	0	0.002	356.0	0	19.6	58.6	0.62	1.16
2.67	74.2	78.8	0	0.002	491.6	0	9.8	81.9	0.83	1.12
									Average:	1.23 %

Table A.3: Filter C 15 cm. Cross angles: 60^o & 30^o. Pore size: 7 mm. Total porosity: 98.3 %

V [m/s]	ΔP [Pa]	$\phi_{effective}$ [%]	K_{in}	K_{out}	F_L [Pa/m]	σ_{in}	σ_{out}	E_{in} [Pa]	RMSE	RMSE/ΔP [%]
1.06	9.8	89.2	1.7	0.022	48.6	0.77	0.001	8.6	0.17	1.71
1.37	16.4	89.4	2.4	0.019	85.6	1.04	0.001	16.0	0.30	1.80
1.68	23.2	89.5	3.8	0.021	118.9	1.40	0.001	23.9	0.39	1.69
1.99	32.6	88.0	4.3	0.002	173.7	1.83	0.001	34.5	0.53	1.63
2.30	45.2	85.3	5.8	0.002	240.1	3.01	0.001	49.0	0.72	1.59
2.62	60.7	85.8	7.8	0.005	323.0	3.83	0.001	66.5	0.94	1.55
2.76	68.0	85.1	8.9	0.005	360.4	4.28	0.001	74.7	1.04	1.53
									Average:	1.64 %

Table A.4: Filter D 15 cm. Cross angles: 75^o & 45^o. Pore size: 7 mm. Total porosity: 98.5 %

V [m/s]	ΔP [Pa]	$\phi_{effective}$ [%]	K_{in}	K_{out}	F_L [Pa/m]	σ_{in}	σ_{out}	E_{in} [Pa]	RMSE	RMSE/ΔP [%]
1.05	5.6	90.9	1.5	0.012	27.1	0.000	0.066	5.0	0.12	2.17
1.36	9.4	88.8	2.7	0.021	45.0	0.000	0.001	10.0	0.24	2.60
1.67	13.0	89.0	3.9	0.019	61.5	0.000	0.001	14.9	0.35	2.71
1.98	17.6	90.8	5.1	0.002	83.2	0.000	0.001	20.9	0.58	3.27
2.30	24.3	89.6	7.4	0.002	113.6	0.000	0.001	29.7	0.77	3.17
2.65	32.5	87.4	9.8	0.005	152.2	0.000	0.001	40.7	1.09	3.34
2.74	37.4	88.6	12.4	0.005	169.7	0.000	0.001	47.3	1.29	3.44
									Average:	2.96 %

Table A.5: Filter D 60 cm. Cross angles: 75^o & 45^o. Pore size: 7 mm. Total porosity: 98.5 %

V [m/s]	ΔP [Pa]	$\phi_{effective}$ [%]	K_{in}	K_{out}	F_L [Pa/m]	σ_{in}	σ_{out}	E_{in} [Pa]	RMSE	RMSE/ΔP [%]
0.44	3.8	74.2	1.2	0.208	7.1	0	0.001	4.2	0.04	1.13
0.76	7.5	87.3	1.8	0.235	9.6	0	0.005	6.7	0.08	0.99
1.06	16.6	82.0	2.8	0.238	18.3	0	0.057	13.4	0.14	0.86
1.38	27.2	81.6	3.7	0.238	27.5	0	0.066	20.5	0.24	0.87
1.67	36.8	81.1	5.4	0.239	35.7	0	0.079	28.0	0.32	0.87
1.99	50.3	80.8	3.9	0.233	51.4	0	0.200	36.8	0.61	1.21
2.31	70.6	79.3	7.5	0.238	68.6	0	0.227	52.1	0.68	0.97
2.60	90.7	79.7	11.4	0.246	84.3	0	0.444	67.0	0.82	0.91
									Average:	0.98 %

Excel files B

The following titles, are the different excel sheets, showing the calculations carried out through this report.

- Filter A, B, C and D (15 and 60 cm)
- Full scale measurement on Mors
- Pressure measurement in filter A 15 cm
- Pressure measurement in filter B 15 cm
- Pressure measurement in filter C 15 cm
- Pressure measurement in filter D 15 cm
- Pressure measurement in filter D 60 cm
- Development and test of the pressure tubes

The excel sheets can be seen on the attached CD.